


# First-principles insights into the high-pressure stability and electronic characteristics of molybdenum nitride

Tao Wang(王涛), Ming-Hong Wen(温铭洪), Xin-Xin Zhang(张新欣), Wei-Hua Wang(王伟华), Jia-Mei Liu(刘佳美), Xu-Ying Wang(王旭颖), and Pei-Fang Li(李培芳)

**Citation:**Chin. Phys. B, 2025, 34 (**3**): 036104. DOI: 10.1088/1674-1056/adab66
Journal homepage: http://cpb.iphy.ac.cn; http://iopscience.iop.org/cpb

**What follows is a list of articles you may be interested in**

---

## Geometries and electronic structures of $Zr_nCu$($n$ =2-12) clusters: A joint machine-learning potential density functional theory investigation

Yizhi Wang(王一志), Xiuhua Cui(崔秀花), Jing Liu(刘静), Qun Jing(井群), Haiming Duan(段海明), and Haibin Cao(曹海宾)
Chin. Phys. B, 2024, 33 (**1**): 016109. DOI: 10.1088/1674-1056/acd5c2

## Pressure-induced phase transition and electronic structure evolution in layered semimetal $HfTe_2$

Mei-Guang Zhang(张美光), Lei Chen(陈磊), Long Feng(冯龙), Huan-Huan Tuo(拓换换), Yun Zhang(张云), Qun Wei(魏群), and Pei-Fang Li(李培芳)
Chin. Phys. B, 2023, 32 (**8**): 086101. DOI: 10.1088/1674-1056/acd2bf

## Probing the effects of lithium doping on structures, properties, and stabilities of magnesium cluster anions

Xiao-Yi Zhang(张小义), Ya-Ru Zhao(赵亚儒), Hong-Xing Li(李红星), Kai-Ge Cheng(成凯格), Zi-Rui Liu(刘子锐), Zhi-Ping Liu(刘芷萍), and Hang He(何航)
Chin. Phys. B, 2023, 32 (**6**): 066102. DOI: 10.1088/1674-1056/acc51f

## Probing structural and electronic properties of divalent metal $Mg_{n+1}$ and $SrMg_n$ ($n$ = 2–12) clusters and their anions

Song-Guo Xi(奚松国), Qing-Yang Li(李青阳), Yan-Fei Hu(胡燕飞), Yu-Quan Yuan(袁玉全), Ya-Ru Zhao(赵亚儒), Jun-Jie Yuan(袁俊杰), Meng-Chun Li(李孟春), and Yu-Jie Yang(杨雨杰)
Chin. Phys. B, 2022, 31 (**1**): 016106. DOI: 10.1088/1674-1056/ac04aa

## Ground-state structure and physical properties of $YB_3$ predicted from first-principles calculations

Bin-Hua Chu(初斌华), Yuan Zhao(赵元), and De-Hua Wang(王德华)
Chin. Phys. B, 2021, 30 (**4**): 046101. DOI: 10.1088/1674-1056/abcf94

---

**SPECIAL TOPIC — Structures and properties of materials under high pressure**

# First-principles insights into the high-pressure stability and electronic characteristics of molybdenum nitride

Tao Wang(王涛)[1], Ming-Hong Wen(温铭洪)[1], Xin-Xin Zhang(张新欣)[2], Wei-Hua Wang(王伟华)[1], Jia-Mei Liu(刘佳美)[1], Xu-Ying Wang(王旭颖)[1], and Pei-Fang Li(李培芳)[1,†]

[1] *Extreme Conditions Physics Research Team, College of Physics and Electronic Information, Inner Mongolia Minzu University, Tongliao* 028043, *China*
[2] *Colledge of Science, Shenyang University of Chemical Technology, Shenyang* 110142, *China*

(Received 17 November 2024; revised manuscript received 16 January 2025; accepted manuscript online 17 January 2025)

Molybdenum nitride, renowned for its exceptional physical and chemical properties, has garnered extensive attention and research interest. In this study, we employed first-principles calculations and the CALYPSO structure prediction method to conduct a comprehensive analysis of the crystal structures and electronic properties of molybdenum nitride ($Mo_xN_{1-x}$) under high pressure. We discovered two novel high-pressure phases: *Imm*2-$MoN_3$ and *Cmmm*-$MoN_4$, and confirmed their stability through the analysis of elastic constants and phonon dispersion curves. Notably, the $MoN_4$ phase, with its high Vickers hardness of 36.9 GPa, demonstrates potential as a hard material. The results of this study have broadened the range of known high-pressure phases of molybdenum nitride, providing the groundwork for future theoretical and experimental researches.

**Keywords:** molybdenum nitride, CALYPSO, crystal structure, high pressure

**PACS:** 61.50.Ks, 71.20.–b

**DOI:** 10.1088/1674-1056/adab66 **CSTR:** 32038.14.CPB.adab66

## 1. Introduction

Transition metal nitrides (TMNs) represent a significant class of functional materials characterized by diverse chemical compositions and structures. They exhibit remarkable physical and chemical properties, including high hardness, excellent thermal stability, good electrical conductivity, and exceptional corrosion resistance. These outstanding properties make TMNs promising candidates for various applications. Their potential applications encompass a wide range of fields, including, but not limited to, catalysis, energy storage, surface coatings, and electromagnetic materials.[1–3] Since Hägg's pioneering investigation on the crystal structure of TMNs,[4] substantial progress has been made in understanding these materials. Sophisticated analytical techniques, including x-ray diffraction, empower researchers to accurately ascertain the crystal structures and atomic configurations of TMNs. This precision facilitates a more profound comprehension of their physicochemical attributes. Moreover, employing structure prediction methodologies aids in the discovery of additional innovative materials with distinctive properties that may be synthesizable. These methods are instrumental in steering the material design and optimization processes.

As an important member of the TMNs, molybdenum nitride was determined to possess a hardness of 44 GPa and a Young's modulus of 605.7 GPa,[5] which is outstanding in the family of TMNs and could be very close to that of diamond and cubic boron nitride. Furthermore, molybdenum nitride boasts a low friction coefficient of 0.07,[6] rendering it an excellent candidate for protective coatings. In terms of electrical properties, molybdenum nitride demonstrates exceptional conductivity and superconducting characteristics. Experimental measurements have documented a conductivity of $1\times10^5$ S/m for $Mo_2N$[7] and an impressive $8.52\times10^5$ S/m for MoN nanosheets.[8] Such conductivity levels position molybdenum nitride as a strong contender for electrode materials in batteries and other electrochemical devices. Additionally, the nanostructured surface and edges of molybdenum nitride offer a plethora of active sites,[9] which significantly enhance its catalytic properties. This feature broadens its potential applications in catalysis.

In 1930, Hägg[4] pioneered the synthesis of molybdenum nitride by employing a method utilizing ammonia and molybdenum powder, and in doing so, identified various crystalline structures of molybdenum nitride, including hexagonal $\delta$-MoN, tetragonal $\beta$-$Mo_{0.72}N_{0.28}$, and cubic $\gamma$-$Mo_2N$. Subsequently, in 1952, Matthias and Hulm[10] experimentally observed a hexagonal-phase molybdenum nitride superconductor with a superconducting transition temperature of around 12.0 K. $\delta1$-MoN was synthesized by Lengauer[11] through the reaction of $MoCl_5$ with ammonia gas at temperatures ranging from 770 K to 1060 K. At 910 K, a hexagonal phase of MoN (space group *P*6*m*2, with lattice parameters $a = 2.851$ Å,

†Corresponding author. E-mail: lipeifang82@163.com

© 2025 Chinese Physical Society and IOP Publishing Ltd. All rights, including for text and data mining, AI training, and similar technologies, are reserved.

$c = 4.782$ Å) was formed, while at 950 K, a cubic $\gamma$-$MoN_{1-x}$ phase began to appear, its proportion increasing with temperature. $\delta$2-MoN was synthesized by Ganin *et al.*[12] at 1003 K through the reaction of $MoCl_5$ with nitrogen, exhibiting a NiAs-type structure with space group $P6_3/mmc$. The lattice parameters were determined to be $a = 2.86$ Å and $c = 5.69$ Å. $\delta$3-MoN was first synthesized by Hägg[4] through the reaction of metallic Mo with ammonia at 973 K. Later, Schönberg[13] employed the same method as Hägg and synthesized molybdenum nitride samples by reacting molybdenum powder with ammonia gas at 1073 K. Schönberg assumed that this hexagonal MoN phase has a space group of $P6_3/mmc$ with lattice parameters $a = 5.725$ Å, $c = 5.608$ Å. In this structure, Mo atoms occupy positions $2b$ (0, 0, 0.25) and $6h$ ($x$, $2x$, 1/4), where $x = 0.489$. Subsequently, Bezinge *et al.*[14] synthesized this hexagonal MoN phase under conditions of 6 GPa and 1800 K, and confirmed the space group as $P6_3/mc$. This structure was also verified by neutron diffraction.[15,16]

Besides the above-mentioned MoN phases, the other molybdenum nitride phases with atomic ratio beyond 1:1 have also been investigated. Troitskaya and Pinsker[17] proposed the existence of a cubic phase $Mo_2N$ with the space group $Pm3m$. Moreover, a hexagonal $Mo_5N_6$ with space group of $P6_3/m$[12] was also identified in their work. In 1970, Ettmayer *et al.*[18] synthesized two distinct phases of $Mo_2N$ from molybdenum nitride powder at 1873 K: a tetragonal phase and a cubic phase. They determined that the tetragonal $Mo_2N$ has the space group of $I4_1/amd$, while the cubic phase $\gamma$-$Mo_2N$ has the space group of $Fm3m$.[19–21] Later, Valeria Tagliazucca *et al.*[22] confirmed the existence of these two cubic phases ($Fm3m$ and $Pm3m$) using x-ray diffraction. The metastable NaCl(B1)-type molybdenum nitride, known for its high superconducting transition temperature, has been identified as a potential high-temperature superconductor. Theoretical studies have predicted a superconducting transition temperature ($T_c$) of around 29 K for this phase.[23–25] Despite many efforts had been made to synthesize the stable NaCl-type molybdenum nitride, only several nitrogen-deficient or vacancy-containing variants were obtained, which might be attributed to its inherent instability, such as the unstable elastic properties[26–28] and thermodynamics.[29] Consequently, the superconducting transition temperature of the synthesized materials still does not reach the expected theoretical values of 20 K to 30 K. In 2015, Shanmin Wang *et al.*[30] synthesized a rhombohedral phase 3R-$MoN_2$, isostructural to $MoS_2$, from a 1:2 molar mixture of $Na_2MoO_4$ and h-BN under a pressure of 3.5 GPa, and identified its space group as $R3m$. This rhombohedral $MoN_2$ phase has been demonstrated to possess good catalytic activity, and its synthetic pressure is suitable for large-scale industrial production. In 2023, Takuya Sasaki *et al.*[31] synthesized a new high-pressure orthorhombic structure $Mo_3N_5$ through the nitriding reaction of molybdenum and nitrogen at pressures exceeding 45 GPa, confirming the space group as $Cmcm$. Most recently, Momoka Demura *et al.*[32] successfully synthesized nitrogen-rich $Mo_2N_3$ at room temperature and pressure using $Na_2MoO_4$ and dicyandiamide precursors.

In 2007, de Paiva and Nogueira[33] conducted a theoretical study on the then-unsynthesized zinc blende structure of molybdenum nitride, employing first-principles methods. They discovered that this structure adopts the space group $F$-$43m$ and has a lattice parameter of 4.58 Å. Given its metallic characteristics, mechanical performance, and paramagnetic properties, this type of structure could potentially be applied in the semiconductor industry or in the production of smooth contact surface films, expanding the range of potential applications of molybdenum nitride compounds. In 2007, Kanoun[34] utilized first-principles methods to perform theoretical calculations on the orthorhombic phase (space groups $F$-$43m$, $Fm3m$, and $Pm3m$) and hexagonal phase ($P6_3/mc$ and $P6m2$) configurations of molybdenum nitride. The calculations indicated that the energy of the cubic phase structures is higher than that of the hexagonal phase structures, suggesting that the hexagonal phase structures are more stable than the cubic phase structures. In 2016, Yu[35] utilized the USPEX crystal structure prediction method to predict different structures of $MoN_2$ at pressures ranging from 0 GPa to 100 GPa. The study determined that the ground state structure of $MoN_2$ is the hexagonal phase nitride with a space group of $P6_3/mmc$. Furthermore, it was found that $MoN_2$ transitions to an orthorhombic phase structure with a space group of $P4/mbm$ at a pressure of 82 GPa. In 2017, Karthik Balasubramanian[36] employed the same methodology to predict the structure of molybdenum nitride. The study identified eight thermodynamically stable structures under ambient pressure, which include $Cm$-MoN, $Cmcm$-$Mo_3N$, $Cm$-$Mo_2N_3$, $P6_3/mmc$-$Mo_3N_2$, $Imm2$-$Mo_4N_3$, $P6_3/mmc$-$MoN_2$ and $Pm3$-$MoN_6$. Balasubramanian noted that under a 1:1 stoichiometric ratio, the monoclinic MoN is the most stable structure, with an energy that is 7 meV lower than that of the hexagonal MoN. In 2018, LiPing Ding *et al.*[37] utilized the CALYPSO program to predict the relevant structures of $MoN_2$ under pressures ranging from 0 GPa to 100 GPa. They discovered a stable orthorhombic $MoN_2$ with a space group of $Cmc21$, which at ambient pressure, has lower energy than the experimentally synthesized rhombohedral $MoN_2$. Furthermore, they observed a transition to an orthorhombic $MoN_2$ structure with a space group of $P12_1/c1$ at a pressure of 25 GPa. In 2019, Qun Wei *et al.*[38] employed the CALYPSO crystal structure prediction method to predict two nitrogen-rich TMNs, $MoN_6$ and $ReN_6$. They found that $MoN_6$ possesses an $Im3m$ space group at 0 GPa. Both materials, $MoN_6$ and $ReN_6$, were identified as potential high-

energy-density materials. Regarding the theoretical study of the structure of molybdenum nitride, while predictions have been made for the binary Mo–N system under ambient conditions and some high pressures, a comprehensive study encompassing all chemical compositions of molybdenum nitride under high pressure has not yet been conducted.

Pressure is a critical thermodynamic variable that has the ability to modify crystal structures, thereby effectively governing material properties. For instance, high-temperature superconductors such as $H_3S$[39] and $LaH_{10}$,[40] which were synthesized under high-pressure conditions, as well as $LaSc_2H_{24}$,[41] a compound predicted through theoretical calculations, have garnered significant attention in the field of materials science. Hence, high pressure provides a unique opportunity to explore and discover novel materials that are not readily available under normal ambient conditions. In conditions of high pressure, interatomic distances are reduced, leading to substantial changes in the properties and strengths of chemical bonds. These modifications hold the promise of creating new materials with increased hardness and stability, potentially leading to advancements in various industries. In TMNs, the covalent and metallic bonds between metal atoms and nitrogen atoms exhibit a synergistic effect, enhancing their overall properties and performance. The strength and directionality of these bonds impart enhanced hardness to the TMNs. Moreover, the electronic coupling between the d electrons of transition metals and the p electrons of nitrogen further strengthens the chemical bond strength, thereby enhancing the material's hardness. For example, $CrN_2$,[42] WN,[43] and MoN[44] all exhibit the characteristic of high hardness. Among them, the hardness of MoN synthesized under high pressure is reported to be 30 GPa.[44] Therefore, exploring the structure of molybdenum nitride under high pressure may lead to the discovery of novel high-hardness materials and previously unknown high-pressure phases that cannot be obtained under normal conditions. The discovery of the new high-pressure orthorhombic structure of $Mo_3N_5$,[31] suggests that there are still many unknown high-pressure phases of molybdenum nitride waiting to be discovered, indicating a vast potential for exploration into novel high-pressure structures.

In this study, we employed the Crystal structure AnaLYsis by Particle Swarm Optimization (CALYPSO) code[45–51] to conduct a global energy minimization structure prediction for the $Mo_xN_{1-x}$ system under different pressures. To determine the dynamical and mechanical stability, we systematically calculated the phonon scattering curves and elastic constants. We also systematically investigated the electronic properties, including the band structure, density of states, electron localization function, and differential charge density, to gain a comprehensive understanding of electronic behavior of the $Mo_xN_{1-x}$ system. The theoretical hardness values were also calculated and the underlying mechanism was analyzed.

## 2. Calculational method

Within the pressure range of 0–100 GPa, we conducted theoretical calculations for the structure prediction of molybdenum nitride, utilizing the CALYPSO method. The accuracy and efficiency of the CALYPSO method in predicting binary and ternary compounds have been extensively evaluated and validated in the literature.[52–57] Density functional theory (DFT),[58] combined with the Perdew–Burke–Ernzerh of generalized gradient approximation (PBE-GGA),[59,60] was used to calculate the initial energy of the structure in the Vinna *ab initio* simulation package (VASP) code.[61] The projector-augmented wave (PAW) method was utilized, employing PAW potentials from the VASP library. The valence electrons considered for the Mo and N atoms were $4s^24p^64d^55s^1$ and $2s^22p^3$, respectively. The energy cutoff of 560 eV was utilized. To ensure enthalpy convergence below 1 meV/atom, Monkhorst–Pack (MP) $k$-point grids of $10\times11\times22$ and $14\times7\times20$ were employed for *Imm*2-$MoN_3$ and *Cmmm*-$MoN_4$, respectively. Additionally, we utilized the Device Studio-projector augmented wave (DS-PAW) software integrated into Device Studio program to calculate the differential charge density, Bader charge, elastic constants and phonon scattering curves.[62] Phonon scattering curves calculations were carried out using the supercell method based on finite displacements.[63] For *Imm*2-$MoN_3$, a supercell of $2\times3\times5$ was used, while for *Cmmm*-$MoN_4$, a supercell of $4\times2\times3$ was utilized.

## 3. Results and discussion

Employing the CALYPSO structure prediction method, we explored the molybdenum nitride ($Mo_xN_{1-x}$) system across a range of stoichiometric ratios and pressures. Through the calculation of enthalpies for compounds with varying ratios, we identified the thermodynamically stable $Mo_xN_{1-x}$ structures. Subsequently, a convex hull diagram was constructed to visualize the most stable structure under each pressure condition. The enthalpy calculation formula used is as follows:

$$\Delta H = [H(\mathrm{Mo}_n\mathrm{N}_m) - nH(\mathrm{Mo}_n) - mH(\mathrm{N}_m)]/(m+n). \quad (1)$$

As depicted in Fig. 1, the solid line represents the lowest energy for a given composition. Consequently, any phase residing above this line is considered thermodynamically unstable, while those lying on the line represent thermodynamically stable phases. The convex hull analysis has identified a total of eight stable $Mo_xN_{1-x}$ phases across the investigated compositions, which include metallic Mo and nitrogen. The

stable phases correspond to the following stoichiometric ratios: $x = 0$, 0.2, 0.25, 0.333, 0.5, 0.5714, 0.6, and 1, These correspond to nitrogen, $MoN_4$, $MoN_3$, $MoN_2$, MoN, $Mo_4N_3$, $Mo_3N_2$, and bcc-Mo.

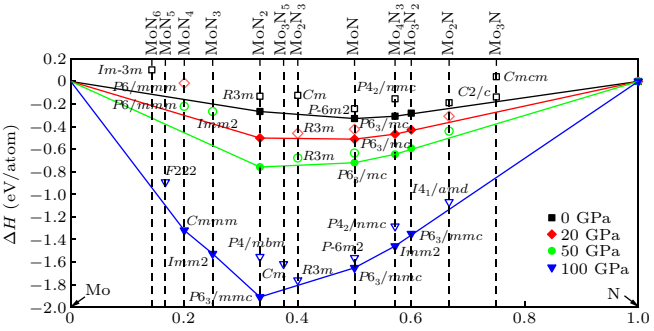



**Fig. 1.** Convex hull diagram for $Mo_xN_{1-x}$ at 0 GPa, 20 GPa, 50 GPa and 100 GPa (solid: stable; open: metastable).

As illustrated in Fig. 1, no phase transitions were observed for the same stoichiometry within the pressure range of 0–100 GPa. The space group for each phase is indicated at the highest pressure of 100 GPa. Under a pressure of 100 GPa, we have predicted the space group of molybdenum nitride (MoN) to be $P6_3/mmc$. However, its stable structure at ambient pressure is $P6_3/mc$. Our calculations have determined the phase transition pressure point to be 71.5 GPa. Furthermore, our predictions indicate that *P*-6*m*2-MoN exhibits a metastable structure within the 0–100 GPa pressure range. This phase is marked in the convex hull diagram at 0 and 100 GPa, with an energy that is 0.087 eV higher compared to the $P6_3/mc$-MoN phase. The ground-state structure of $MoN_2$ predicted in our study is $P6_3/mmc$, which is consistent with the results obtained by Yu *et al.*[35] At 100 GPa, our analysis did not detect any phase transitions. However, at this pressure, we also predicted the existence of the $P4/mbm$-$MoN_2$ phase, which is less stable with an energy 0.356 eV higher than that of the $P6_3/mmc$-$MoN_2$ phase. Furthermore, we also discovered two additional phases: *P*-6*m*2-$MoN_2$ and *R*3*m*-$MoN_2$. The *P*-6*m*2-$MoN_2$ phase is only 9 meV higher in energy than the $P6_3/mmc$-$MoN_2$ phase, indicating its potential for stability under certain conditions. We predicted that the $P6_3/mmc$-$Mo_3N_2$ phase exhibits thermodynamic stability, which is consistent with the $Mo_3N_2$ structure reported by Karthik Balasubramanian.[36] Additionally, we confirmed the thermodynamic stability of the *Imm*2-$Mo_4N_3$ structure under high pressure, as proposed by Karthik Balasubramanian. Notably, at 100 GPa, we identified two new stable structures: *Imm*2-$MoN_3$ and *Cmmm*-$MoN_4$. The phase diagram of the aforementioned structure is shown in Fig. 2.

Beyond the stable structures previously discussed, our research has also predicted the existence of several metastable molybdenum nitride structures across the pressure range of 0–100 GPa. Both $Mo_2N_3$ and $Mo_2N$ displayed metastable phases within this range. Notably, the *R*3*m*-$Mo_2N_3$ phase was found to be in a metastable state at 100 GPa, with an energy just 0.045 eV above the convex hull. Furthermore, at ambient pressure, we identified a *C*2/*c*-$Mo_3N$ structure in a metastable state, with an energy of only 0.042 eV above the convex hull. These metastable phases offer insights into potential new stable structures under different pressures, enhancing our understanding of molybdenum nitride's high-pressure behavior.

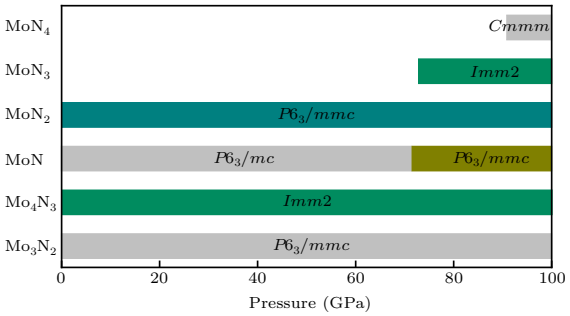



**Fig. 2.** Pressure–composition phase diagrams of the stable $Mo_xN_{1-x}$ structures.

Figure 3 displays the crystal structures of *Cmmm*-$MoN_4$ and *Imm*2-$MoN_3$, with their optimized lattice parameters listed in Table 1. In Fig. 3(a), the C*mmm*-$MoN_4$ structure features each Mo atom coordinated with eight N atoms, creating a stable and tightly bound environment. Stable Mo–N bonds form between Mo and N atoms, with a length of 2.07 Å and angles of 63.51°, 73.2°, and 74.6° between adjacent bonds, indicating stable metal–nonmetal interactions. This structure also incorporates N–N bonds, measuring 1.37 Å in length. The presence of these N–N bonds, coupled with the eightfold coordination around Mo atoms and the high-symmetry orthorhombic structure, results in a highly ordered atomic arrangement. This high-symmetric structure reduces stress concentration, leading to a uniform distribution of bond strength throughout the crystal. Such even bonding enhances the structural stability, conferring high compressive strength and resistance to localized deformation. These characteristics indicate that *Cmmm*-$MoN_4$ is likely to possess high hardness and favorable mechanical properties.

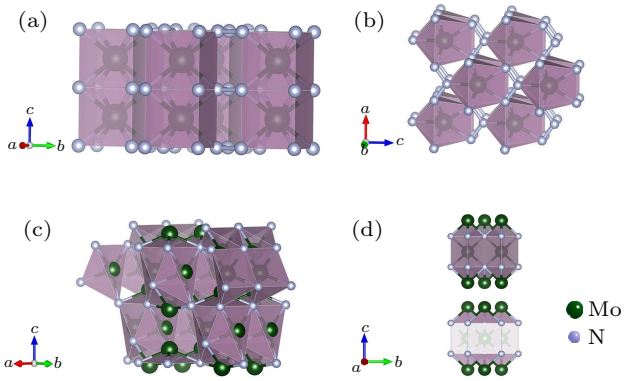



**Fig. 3.** Crystal structures of $Mo_xN_{1-x}$: (a) *Cmmm* phase of $MoN_4$, (b) *Imm*2 phase of $MoN_3$, (c) *Imm*2 phase of $Mo_4N_3$, (d) $P6_3/mmc$ phase of $Mo_3N_2$.

**Table 1.** Lattice parameters and atomic Wyckoff positions of $MoN_3$ and $MoN_4$.

| Structures | Pressure (GPa) | Lattice parameters (Å) | Atoms | | Wyckoff positions (fractional) | | |
|---|---|---|---|---|---|---|---|
| | | | | | *x* | *y* | *z* |
| *Imm*2 | 100 | $a = 5.13$ | Mo1 | 2*a* | 0.00 | 0.00 | 0.04 |
| ($MoN_3$) | | $b = 2.51$ | N1 | 4*c* | 0.79 | 0.00 | 0.43 |
| | | $c = 4.48$ | N2 | 2*a* | 0.00 | 0.00 | 0.60 |
| *Cmmm* | 100 | $a = 3.00$ | Mo1 | 2*b* | 0.50 | 0.00 | 0.00 |
| ($MoN_4$) | | $b = 7.54$ | N1 | 8*q* | 0.81 | 0.16 | 0.50 |
| | | $c = 2.51$ | | | | | |

Figure 3(b) illustrates the *Imm*2-$MoN_3$ structure, characterized by a polyhedral stacking arrangement. Each Mo atom is coordinated with seven N atoms, with Mo–N bond lengths averaging around 2.0 Å and N–N bonds are present, measuring 1.31 Å in length. The stacking consists of edge-sharing heptagonal polyhedra and N–N bonds. The presence of edge-sharing polyhedra is a common feature in materials with high thermal and chemical stability, suggesting that the *Imm*2-$MoN_3$ structure may exhibit these attributes as well.

To elucidate the bonding characteristics within various molybdenum nitride compounds, we computed the electronic localization function (ELF), as depicted in Fig. 4. In the $MoN_3$ structure, the ELF values between adjacent Mo and N atoms are 0.41 and 0.47, respectively. For the $MoN_4$ structure, the ELF value between neighboring Mo and N atoms is 0.34, whereas the ELF value between adjacent N atoms is notably higher at 0.85, signifying the presence of a typical covalent bond between these neighboring nitrogen atoms.

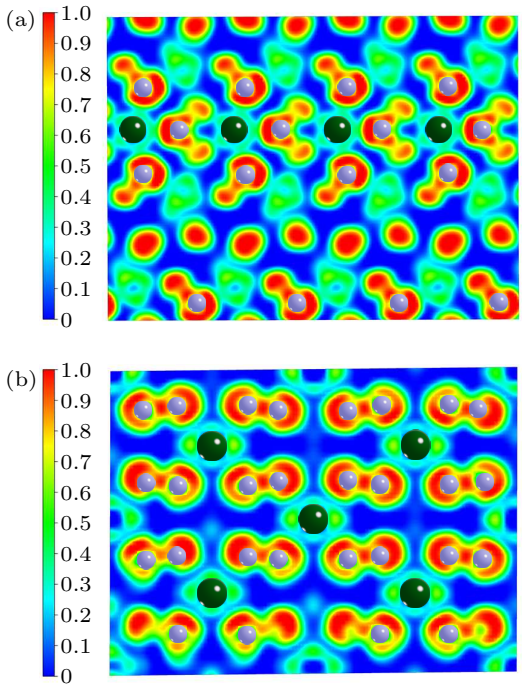



**Fig. 4.** Electronic localization function of $MoN_3$ and $MoN_4$: (a) *Imm*2 phase of $MoN_3$, (b) *Cmmm* phase of $MoN_4$.

To deepen our understanding of the characteristics of molybdenum nitrides, we conducted a comprehensive analysis of their electronic properties. This included calculations of the band structure, density of states, charge density difference, and Bader charge. Figure 5 illustrates the electronic band structures and DOS for the compounds $MoN_3$ and $MoN_4$. The band structures demonstrate that both materials possess bands that cross the Fermi level, indicative of metallic properties. At the Fermi level, the DOS is predominantly contributed by the Mo-4d and N-2p orbitals.

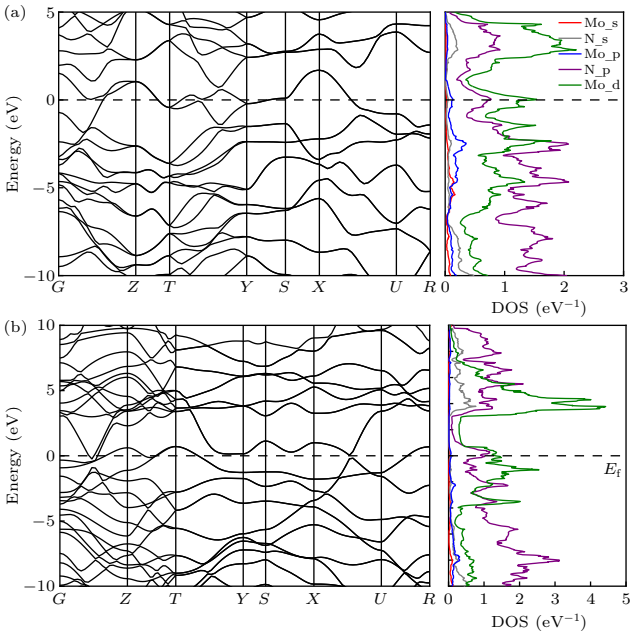



**Fig. 5.** Electronic band structures (left panel) and partial density of state (right panel) for $Mo_xN_{1-x}$ based on the analysis: (a) *Imm*2 phase of $MoN_3$, (b) *Cmmm* phase of $MoN_4$.

**Table 2.** The simulated Bader charge of $MoN_3$ and $MoN_4$.

| | Mo | N1 | N2 | N3 | N4 |
|---|---|---|---|---|---|
| $MoN_3$ | 12.22 | 5.76 | 5.76 | 5.26 | |
| $MoN_4$ | 12.43 | 5.49 | 5.29 | 5.25 | 5.54 |

Figure 6 presents the charge difference density for $MoN_3$ and $MoN_4$, with yellow indicating regions of charge accumulation and blue denoting areas of charge depletion. The visualization clearly shows an electron transfer from Mo to N atoms. To quantify this transfer, Bader charge analysis was conducted for both compounds, and the results are summarized in Table 2. Taking into account the valence electrons of Mo, which is 14, and N, which is 5, in the $MoN_3$ unit cell, Mo atoms lose a total of 3.14 electrons, which are acquired by N atoms.

Similarly, in the $MoN_4$ unit cell, Mo atoms lose a total of 3.56 electrons, which are gained by N atoms.

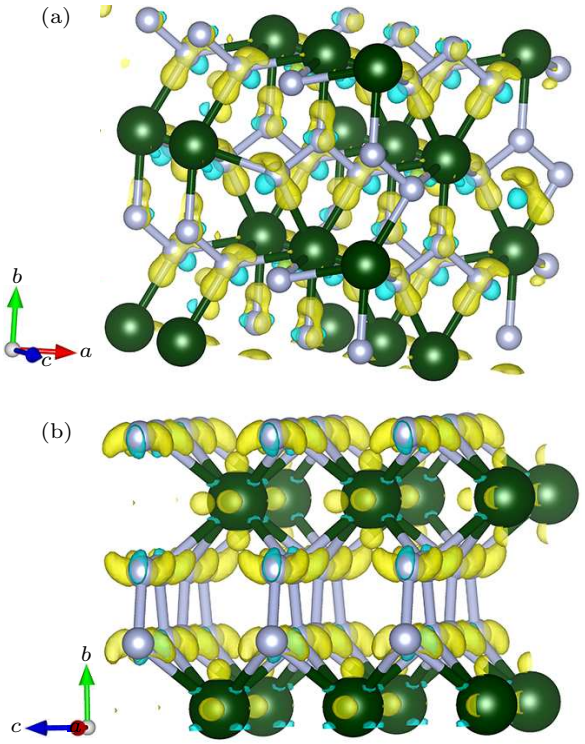



**Fig. 6.** The calculated charge density: (a) *Imm*2 phase of $MoN_3$, (b) *Cmmm* phase of $MoN_4$.

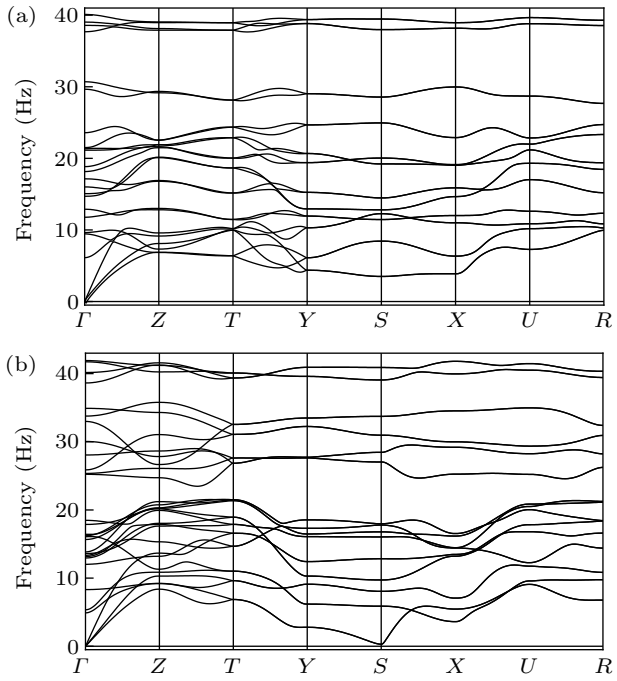



**Fig. 7.** Phonon dispersion curves for (a) *Imm*2 phase of $MoN_3$ and (b) *Cmmm* phase of $MoN_4$.

To determine the stability of $MoN_3$ and $MoN_4$, we calculated their phonon dispersion curves and elastic constants. Utilizing the finite displacement method, we obtained the phonon dispersion curves for the *Imm*2-$MoN_3$ and *Cmmm*-$MoN_4$ structures, which are crucial for evaluating dynamic stability. Figure 7 displays the phonon dispersion curves for both $MoN_3$ and $MoN_4$, with the notable absence of imaginary frequencies across the entire Brillouin zone, thereby confirming the dynamic stability of both structures.

The mechanical stability of a crystal structure is determined by specific criteria that depend on the crystal system. For the orthorhombic *Imm*2-$MoN_3$ and *Cmmm*-$MoN_4$ structures, the elastic constants must meet the following conditions to ensure mechanical stability:[64]

$$C_{11}>0,\ C_{22}>0,\ C_{33}>0,\ C_{44}>0,\ C_{55}>0,\ C_{66}>0, \quad (2)$$

$$C_i=[C_{11}+C_{22}+C_{33}+2(C_{12}+C_{13}+C_{23})]>0, \quad (3)$$

$$C_j=(C_{11}+C_{22}-2C_{12})>0, \quad (4)$$

$$C_k=(C_{11}+C_{33}-2C_{13})>0, \quad (5)$$

$$C_l=(C_{22}+C_{33}-2C_{23})>0. \quad (6)$$

The elastic constants for the *Imm*2-$MoN_3$ and *Cmmm*-$MoN_4$ structures were determined employing the strain–stress method, with the findings presented in Table 3. The analysis of these results demonstrates that both structures comply with the necessary stability criteria, thereby validating their mechanical stability.

Table 3 summarizes the elastic constants for several high-hardness materials and nitrides.[65–70] The findings reveal that *Cmmm*-$MoN_4$ possesses large elastic constants $C_{11}$, $C_{22}$, and $C_{33}$, which indicate a significant resistance to compression along the axial direction. Particularly, the elastic constant $C_{11}$ is 1437.2 GPa, which is comparable to the elastic constant of c-BN under 100 GPa pressure, approximately 1500 GPa.[71] At normal pressure, it is 779 GPa,[66] suggesting an extremely high incompressibility along the *a*-axis. According to the data presented in Table 3, the $B/G$ ratios for high-hardness materials such as diamond typically fall below 1.75, which is indicative of their brittle nature. However, the computed $B/G$ ratio for *Imm*2-$MoN_3$ is 2.38, suggesting ductile behavior. In contrast, *Cmmm*-$MoN_4$ exhibits a $B/G$ value of 1.57, which is below 1.75 and situated between the values of WN (1.643)[68] and AlN (1.1),[69] thus classifying it as a brittle material. Consequently, *Cmmm*-$MoN_4$ is likely to possess higher hardness.

The material's high hardness is likely attributed to its high bulk modulus, shear modulus, low Poisson's ratio, and strong covalent bonding. Utilizing the VRH approximation,[72] we obtained the bulk modulus ($B$), shear modulus ($G$), Young's modulus ($E$), and Poisson's ratio ($\nu$), where the three-dimensional images of *Imm*2-$MoN_3$ and *Cmmm*-$MoN_4$ are shown in Figs. 8 and 9, respectively. *Imm*2-$MoN_3$ and *Cmmm*-$MoN_4$ exhibit anisotropic mechanical properties, with a higher modulus in the [100]–[010] plane relative to the [001] direction. *Imm*2-$MoN_3$ demonstrates the highest bulk modulus of 1195 GPa in the [100] direction. The bulk modulus of *Cmmm*-

$MoN_4$ exhibits isotropy within the [100]–[010] plane, achieving a notably high value of 796 GPa, which underscores its significant resistance to compression. In contrast, the bulk modulus in the [001] direction is considerably lower, at 426 GPa. Based on the data presented in Table 3, it is evident that $MoN_4$ exhibits a higher Young's modulus and shear modulus in comparison to $MoN_3$. The ranges of shear modulus and Young's modulus for *Cmmm*-$MoN_4$ are 351 GPa–586 GPa and 716 GPa–1353 GPa, respectively. The high Young's modulus in the [100]–[010] plane also indicates that it has a strong resistance to tensile deformation within its elastic deformation range, and the highest value of shear modulus in this plane corresponds to the lowest value of Young's modulus. Poisson's ratio measures the expansion or contraction sideways that occurs when a material is stretched or compressed.[73] The Poisson's ratio of *Cmmm*-$MoN_4$ is estimated to range from 0.22 to 0.40, with a big lateral expansion occurring at the angle between the [100] and [001] directions. Meanwhile, *Imm*2-$MoN_3$ also demonstrates a relatively significant lateral expansion in the [100] direction. The elastic constant results suggest that *Cmmm*-$MoN_4$ have the potential to be a hard materials. Consequently, we calculated their Vickers hardness. The formula is as follows:[74]

$$H_v\ (\text{GPa}) = 2(K^2G)^{0.585} - 3, \tag{7}$$

where $K = G/B$ is Pugh's modulus ratio.

**Table 3.** The elastic constants, bulk modulus $B$ (GPa), shear modulus $G$ (GPa), Young's modulus $E$ (GPa) and Poisson's ratio $\nu$ of $MoN_3$, $MoN_4$, and other high-hardness materials or nitrides.

| | Pressure | $C_{11}$ | $C_{22}$ | $C_{33}$ | $C_{44}$ | $B$ | $G$ | $E$ | $\nu$ |
|---|---|---|---|---|---|---|---|---|---|
| $MoN_3$ | 100 | 1309.4 | 1287.7 | 778.5 | 118.4 | 577.0 | 247.8 | 650.4 | 0.31 |
| $MoN_4$ | 100 | 1437.2 | 1208.5 | 930.7 | 351.4 | 610.3 | 396.0 | 976.8 | 0.23 |
| Diamond[a] | 0 | 1074.8 | | | 720.6 | 442 | 609.5 | 1048.5 | 0.1 |
| c-BN[b] | 0 | 779 | | | 446 | 370 | 384 | 856 | 0.12 |
| Zb-BN[c] | 0 | 812 | | | 462.9 | 389.7 | 401 | 890.4 | 0.11 |
| NiAs-WN[d] | 0 | 650.2 | | 800.6 | 281.9 | 396 | 241 | 602 | 0.25 |
| AlN[e] | 40 | 800.4 | | | 419.4 | 402.9 | 365.9 | 842.4 | 0.15 |
| $YN_2$[f] | 100 | 346.5 | 346.8[f] | 162.3 | 55.0 | 115.9 | 70.9 | 176.7 | 0.25 |
| $Y_2N$[f] | 100 | 173.0 | 175.3[f] | 164.4 | −243.9 | 82.6 | 43.2 | 110.3 | 0.28 |

[a]Ref. [65], [b]Ref. [66], [c]Ref. [67], [d]Ref. [68], [e]Ref. [69], [f]Ref. [70].

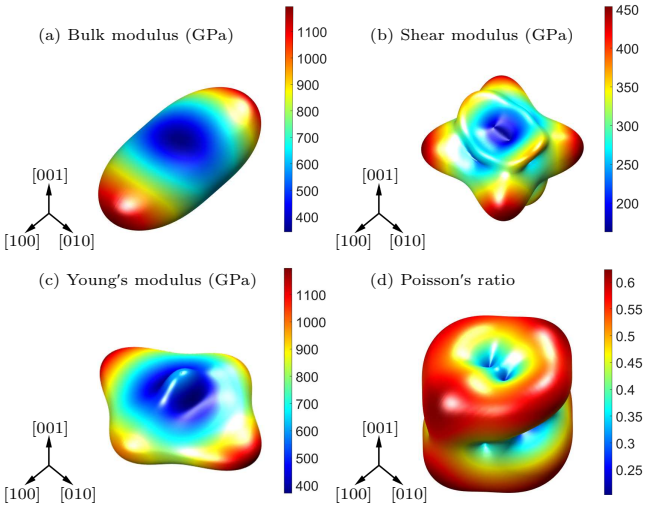



**Fig. 8.** (a) Bulk modulus, (b) shear modulus, (c) Young's modulus and (d) Poisson's ratio of *Imm*2-$MoN_3$ in three dimensions.

At a pressure of 100 GPa, the Vickers hardness of *Imm*2-$MoN_3$ is measured at 15.7 GPa, whereas *Cmmm*-$MoN_4$ exhibits a significantly higher hardness of 36.9 GPa, positioning it within the realm of hard materials and nearing the threshold for superhard materials. When compared to $MoN_3$, $MoN_4$ demonstrates a higher bulk modulus, shear modulus, and a lower Poisson's ratio, which underscores the importance of these properties in determining material hardness. These mechanical properties contribute significantly to the material's resistance to deformation and its ability to withstand compressive and tensile stresses, thereby influencing its overall hardness and potential applications in various industrial sectors.

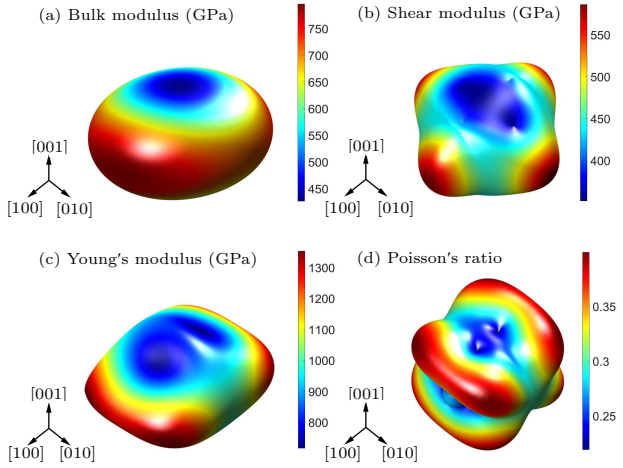



**Fig. 9.** (a) Bulk modulus, (b) shear modulus, (c) Young's modulus and (d) Poisson's ratio of *Cmmm*-$MoN_4$ in three dimensions.

## 4. Conclusion

The CALYPSO method was utilized to forecast the crystal structures of molybdenum nitride ($Mo_xN_{1-x}$) under high-pressure conditions, which led to the discovery of two new

structures: *Imm*2-$MoN_3$ and *Cmmm*-$MoN_4$. The stability, electronic properties, and hardness of these two structures were studied using first-principles methods. Elastic constants and phonon dispersion curves indicate that both structures are mechanically and dynamically stable. The band structure and density of states show that both structures exhibit metallic behavior, with the density of states at the Fermi level predominantly contributed by Mo-4d and N-2p orbitals. *Cmmm*-$MoN_4$ demonstrates a higher bulk modulus and Young's modulus, signifying its strong resistance to compression and tensile deformation. The Vickers hardness calculation indicates that *Cmmm*-$MoN_4$ possesses a hardness of 36.9 GPa, suggesting its potential as a candidate for hard materials.

## Acknowledgments

Project supported by the National Natural Science Foundation of China (Grant No. 11964026), the Natural Science Foundation of Inner Mongolia, China (Grant Nos. 2019MS01010 and 2023LHMS01014), Higher Educational Scientific Research Projects of Inner Mongolia (Grant Nos. NJZZ19145 and NJZZ22470), the Educational Scientific Research Project of Liaoning Province (Grant No. LJKZ0452), the Doctoral Starting up Foundation of Inner Mongolia Minzu University of Science and Technology (Grant No. BSZ023), Inner Mongolia Autonomous Region Youth Capacity Improvement Project (Grant No. GXKY22157), and Higher Physics Major Teaching Steering Committee of the Ministry of Education Project (Grant No. JZW-23-GT-21). We gratefully acknowledge HZWTECH for providing computation facilities.

## References

[1] Zeng R, Li H Q, Shi Z X, Meng J H, Xu W X, Wang H S, Li Q H, Pollock C J, Lian T Q, Mavrikakis M, Muller D A and Abruña H D 2024 *Nat. Mater.* **23** 1695
[2] Zhong Y, Xia X H, Shi F, Zhan J Y, Tu J P and Fan H J 2016 *Adv. Sci.* **3** 1500286
[3] Theerthagiri J, Lee S J, Murthy A P, Madhavan J and Choi M Y 2020 *Curr. Opin. Solid State Mater.* **24** 100805
[4] Hägg G Z 1930 *Phys. Chem. B* **7** 339
[5] Krysina O V, Shugurov V V, Koval N and Prokopenko N 2016 *Key Eng. Mater.* **712** 9
[6] Bondar O V, Postol'nyi B A, Beresnev V M, Abadias G, Chartier P, Sobol O V, Kolesnikov D A, Komarov F F, Lisovenko M O and Andreev A A 2015 *J. Superhard Mater.* **37** 27
[7] Jiang G S, Xu F, Yang S H, Wu J P, Wei B Q and Wang H Q 2018 *J. Power Sources* **395** 77
[8] Wang Y Q, Jian C Y, Hong W T and Liu W 2021 *Chem. Commun.* **57** 223
[9] Xie J F, Li S, Zhang X D, Zhang J J, Wang R X, Zhang H, Pan B C and Xie Y 2014 *Chem. Sci* **5** 4615
[10] Matthias B T and Hulms J K 1952 *Phys. Rev.* **87** 799
[11] Lengauer W 1988 *J. Cryst. Growth* **87** 295
[12] Ganin A Y, Kienle L and Vajenine G V 2006 *J. Solid State Chem.* **179** 2339
[13] Schönberg N 1954 *Acta Chem. Scand.* **8** 204
[14] Bezinge A, Yvon K, Muller J, Lengaeur W and Ettmayer P 1987 *Solid State Commun.* **63** 141
[15] Marchand R, Tessier F and DiSalvo F J 1999 *J. Mater. Chem.* **9** 297
[16] Bull C L, McMillan P F, Soignard E and Leinenweber K 2004 *J. Solid State Chem.* **177** 1488
[17] Troitskaya N V and Pinsker Z G 1959 *Sov. Phys. Crystallogr.* **1959** 33
[18] Ettmayer P 1970 *Monatsh. Chem.* **101** 127
[19] Zhao E J, Wang J P and Wu Z J 2010 *Phys. Status Solidi B* **247** 1207
[20] Anitha V P, Major S, Chandrashekharam D and Bhatnagar M 1996 *Surf. Coat. Technol.* **79** 50
[21] Bull C L, Kawashima T, McMillan P F, Machon D, Shebanova O, Daisenberger D, Soignard E, Takayama-Muromachi E and Chapon L C 2006 *J. Solid State Chem.* **179** 1762
[22] Tagliazucca V, Leonib M and Weidenthaler C 2014 *Phys. Chem. Chem. Phys.* **16** 21882
[23] Pickett W E, Klein B M and Papaconstantopoulos D A 1981 *Physica B & C* **107** 667
[24] Papaconstantopoulos D A, Pickett W E, Klein B M and Boyer L L 1985 *Phys. Rev. B* **31** 752
[25] Zhao Y X and He S A 1983 *Solid State Commun.* **45** 281
[26] Chen J, Boyer L L, Krakauer H and Mehl M J 1988 *Phys. Rev. B* **37** 3295
[27] Hart G W and Klein B M 2000 *Phys. Rev. B* **61** 3151
[28] Kanoun M B, Goumri-Said S and Jaouen M 2007 *Phys. Rev. B* **76** 134109
[29] Isaev E I, Simak S I, Abrikosov I A, Ahuja R, Vekilov Y K, Katsnelson M I and Lichtenstein A I 2007 *J. Appl. Phys.* **101** 123519
[30] Wang S M, Ge H, Sun S L, Zhang J Z, Liu F M, Wen X D, Yu X H, Wang L Q, Zhang Y, Xu H W, Neuefeind J C, Qin Z F, Chen C F, Jin C Q, Li Y W, He D W and Zhao Y S 2015 *J. Am. Chem. Soc.* **137** 4815
[31] Sasaki T, Yamamoto T, Asano S, Niwa K and Hasegawa M 2023 *Dalton Trans.* **52** 469
[32] Demura M, Nagao M, Lee C, Goto Y, Avdeev M, Masubuchi Y J, Mitsudome T, Sun W, Tasanaga K and Miura A 2024 *Inorg. Chem.* **63** 4989
[33] Paiva R D and Nogueira R A 2007 *Phys. Rev. B* **75** 085105
[34] Kanoun M B, Goumri-Said S and Jaouen M 2007 *Phys. Rev. B* **74** 134109
[35] Yu S Y, Huang B W, Jia X J, Zeng Q F, Oganov A R, Zhang L T and Frapper G 2016 *Phys. Chem. C* **120** 11060
[36] Balasubramanian K, Huang L P and Gall D 2017 *J. Appl. Phys.* **122** 195101
[37] Ding L P, Shao P, Zhang F H, Lu C and Huang X F 2018 *Phys. Chem. C* **122** 21039
[38] Wei Q, Zhao C Y, Zhang M G, Yan H Y and Wei B 2019 *Phys. Lett. A* **383** 2429
[39] Drozdov A P, Eremets M I, Troyan I A, Ksenofontov V and Shylin S I 2015 *Nature* **525** 73
[40] Drozdov A P, Kong P P, Minkov V S, Besedin S P, Kuzovnikov M A, Mozaffari, S, Balicas L, Balakirev F F, Graf D E, Prakapenka V B, Greenberg E, Knyazev D A, Tkacz M and Eremets M I 2019 *Nature* **569** 528
[41] He X L, Zhao W B, Xie Y, Hermann A, Hemley R J, Liu H H and Ma Y M 2024 *Proc. Natl. Acad. Sci. USA* **121** e2401840121
[42] Zhao Z L, Bao K, Tian F B, Duan D F, Liu B B and Cui T 2016 *Phys. Rev. B* **93** 214104
[43] Xia K, Gao H, Liu C, Yuan, J N, Sun J, Wang H T and Xing D Y 2018 *Sci. Bull.* **63** 817
[44] Wang S M, Antonio D, Yu X H, Zhang J Z, Cornelius A L, He D W and Zhao Y S 2015 *Sci. Rep.* **5** 13733
[45] Wang Y, Lv J, Zhu L and Ma Y 2010 *Phys. Rev. B* **82** 094116
[46] Wang Y, Lv J, Zhu L and Ma Y 2012 *Comput. Phys. Commun.* **183** 2063
[47] Lu C, Gong W, Li Q and Chen C 2020 *J. Phys. Chem. Lett.* **11** 9165
[48] Zhang L J, Wang Y C, Lv J and Ma Y M 2017 *Nat. Rev. Mater.* **2** 1
[49] Wang Y and Ma Y 2014 *J. Chem. Phys.* **140** 040901
[50] Lu C, Li Q, Ma Y and Chen C 2017 *Phys. Rev. Lett.* **119** 115503
[51] Li Y, Wang Y, Pickard C J, Needs R J, Wang Y and Ma Y 2015 *Phys. Rev. Lett.* **114** 125501
[52] Li P F, Lang H Y, Bao X, Feng C S, Xing S Y, Lin J Y and Ma X J 2022 *Comp. Mater. Sci.* **207** 111310
[53] Bao X, Lang H Y, Ma X J, Ou T J, Zhang M G, Zhang X X and Li P F 2022 *Solid State Commun.* **342** 114635
[54] Liu G T, Wang H, Ma Y M and Ma Y M 2011 *Solid State Commun.* **151** 1899
[55] Hamlin J J 2015 *Phys. C* **514** 59

[56] Eberhart R and Kennedy J 1995 *Proceedings of the Sixth International Symposium on Micro Machine and Human Science*, October 4–6, 1995, Nagoya, Japan, p. 39
[57] Kennedy J and Eberhart R 1995 *Proceedings of ICNN'95-international conference on neural networks*, November 27–December 01, 1995, Perth, Australia, p. 1942
[58] Perdew J P, Chevary J A, Vosko S H, Jackson K A, Pederson M R, Singh D J and Fiolhais C 1992 *Phys. Rev. B* **46** 6671
[59] Perdew J P, Burke K and Ernzerhof M 1996 *Phys. Rev. Lett.* **77** 3865
[60] Fu X, Fonrose W, Arras R, Demaille D, Eddrief M and Etgens V 2015 *Appl. Phys. Lett.* **125** 89
[61] Kresse G and Furthmüller J 1996 *Phys. Rev. B* **54** 11169
[62] Blochl P E 1994 *Phys. Rev. B* **50** 17953
[63] Togo A, Oba F and Tanaka I 2008 *Phys. Rev. B* **78** 134106
[64] Mouhat F and Coudert F X 2014 *Phys. Rev. B* **90** 224104
[65] Guler E and Gueler M 2015 *Chin. J. Phys.* **53** 195
[66] Zhang Q D, Zou Y C, Fan Q Y and Yang Y T 2020 *Materials* **13** 1280
[67] Fatmi M, Ghebouli B, Ghebouli M A and Hieba Z K 2011 *Phys. Scr.* **83** 065702
[68] Qin J Q, Zhang X Y, Xue Y N, Li X T, Ma M Z and Liu R P 2013 *Comput. Mater. Sci.* **79** 456
[69] Zagorac D, Zagorac J, Djukic M B, Jordanov D and Matovic B 2019 *Theor. Appl. Fract. Mech.* **103** 102289
[70] Wang F X, Rui Q, Jiang Q W, Li J F, Zhu H Y, Wang Q L and Wang X L 2022 *Solid State Commun.* **358** 115001
[71] Guo Y D, Yang X D, Li X B, Song X S and Cheng X L 2008 *Diamond Relat. Mater.* **17** 1
[72] Hill R 1952 *Proc. Phys. Soc. A* **65** 349
[73] Ding S C, Wang S, Liu Y, Zurek E, Zhu L and Yang G C 2024 *J. Am. Chem. Soc.* **146** 34466
[74] Chen X Q, Niu H Y, Li D Z and Li Y Y 2011 *Intermetallics* **19** 1275